

Micromachined three-dimensional electrode arrays for transcutaneous nerve tracking

This article has been downloaded from IOPscience. Please scroll down to see the full text article.

2011 J. Micromech. Microeng. 21 085014

(<http://iopscience.iop.org/0960-1317/21/8/085014>)

View [the table of contents for this issue](#), or go to the [journal homepage](#) for more

Download details:

IP Address: 130.207.50.192

The article was downloaded on 02/08/2011 at 15:15

Please note that [terms and conditions apply](#).

Micromachined three-dimensional electrode arrays for transcutaneous nerve tracking

Swaminathan Rajaraman^{1,2}, Julian A Bragg^{3,4}, James D Ross^{2,5}
and Mark G Allen¹

¹ School of Electrical and Computer Engineering, Georgia Institute of Technology, Atlanta, GA, USA

² Axion BioSystems Inc., Atlanta, GA, USA

³ Department of Neurology, Emory University, Atlanta, GA, USA

⁴ Midtown Neurology, Atlanta, GA, USA

⁵ Wallace H Coulter Department of Biomedical Engineering, Georgia Tech/Emory University, Atlanta, GA, USA

E-mail: srajaraman@axionbio.com

Received 3 March 2011, in final form 2 May 2011

Published 30 June 2011

Online at stacks.iop.org/JMM/21/085014

Abstract

We report the development of metal transfer micromolded (MTM) three-dimensional microelectrode arrays (3D MEAs) for a transcutaneous nerve tracking application. The measurements of electrode–skin–electrode impedance (ESEI), electromyography (EMG) and nerve conduction utilizing these minimally invasive 3D MEAs are demonstrated in this paper. The 3D MEAs used in these measurements consist of a metalized micro-tower array that can penetrate the outer layers of the skin in a painless fashion and are fabricated using MTM technology. Two techniques, an inclined UV lithography approach and a double-side exposure of thick negative tone resist, have been developed to fabricate the 3D MEA master structure. The MEAs themselves are fabricated from the master structure utilizing micromolding techniques. Metal patterns are transferred during the micromolding process, thereby ensuring reduced process steps compared to traditional silicon-based approaches. These 3D MEAs have been packaged utilizing biocompatible Kapton[®] substrates. ESEI measurements have been carried out on test human subjects with standard commercial wet electrodes as a reference. The 3D MEAs demonstrate an order of magnitude lower ESEI (normalized to area) compared to wet electrodes for an area that is 12.56 times smaller. This compares well with other demonstrated approaches in literature. For a nerve tracking demonstration, we have chosen EMG and nerve conduction measurements on test human subjects. The 3D MEAs show 100% improvement in signal power and $\text{SNR}/\sqrt{\text{area}}$ as compared to standard electrodes. They also demonstrate larger amplitude signals and faster rise times during nerve conduction measurements. We believe that this microfabrication and packaging approach scales well to large-area, high-density arrays required for applications like nerve tracking. This development will increase the stimulation and recording fidelity of skin surface electrodes, while increasing their spatial resolution by an order of magnitude or more. Although biopotential electrode systems are not without their challenges, the non-invasive access to neural information, along with the potential for automation with associated electronic and software development, is precisely what makes this technology an excellent candidate for the next generation in diagnostic, therapeutic, and prosthetic devices.

(Some figures in this article are in colour only in the electronic version)

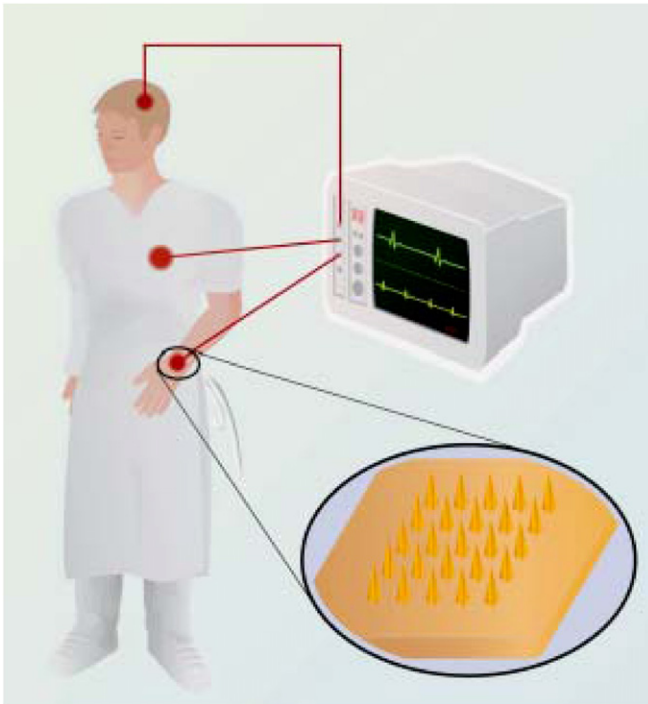


Figure 1. This figure summarizes the opportunities for biopotential electrodes in a clinical setting: EMG, ECG and EEG are all applications where standard biopotential electrodes are used. The inset on the right-hand side provides a schematic of the proposed micromachined 3D MEAs to replace the standard surface electrodes.

1. Introduction

The ability to precisely sense and manipulate the human nervous system without invasively entering the body would enable major advances in neural prosthetics [1], therapeutic stimulation [2, 3], and clinical diagnostics [4]. Although classical interfaces—such as those used for electromyography (EMG), electrocardiography (ECG), nerve conduction studies (NCS) [5], etc—provide a foundation for such a non-invasive neural interaction, they are limited by three major constraints: (1) signals generated by traditional biopotential electrodes suffer from high noise levels and low spatial resolution, (2) surface stimulation temporarily induces ‘blind spots’ or artifacts that obscure evoked responses, and (3) anatomical variations between patients render traditional electrode placement unpredictable [4, 9]. While researchers and physicians are able to partially overcome these shortcomings through training and effort, they quickly encounter fundamental limits to the precision with which they can evaluate and control electroactive tissue. Figure 1 summarizes opportunities for biopotential electrodes (for nerve tracking and other applications) in the human body. The inset has the schematic of the proposed electrode system which is described later in this section.

The non-invasive nature of bioelectrodes is also directly responsible for its most significant shortcomings—low spatial resolution and poor signal-to-noise (SNR) ratios [4]. This complication arises because non-invasive electrodes sit atop high-impedance skin tissue that impedes the propagation of

electrical signals. Specifically, the outermost layer of the skin, the stratum corneum (SC), is composed of dead skin cells that act as a fluid barrier and possess electrical isolation characteristics [6]. Therefore, in order to ensure minimal signal attenuation and noise inference, it is critical to lower the skin interface impedance [7, 8]. This is especially true for stimulation and recording applications, in which high skin impedance not only diminishes the recording signals but also requires much higher, potentially painful, stimuli.

Today, the most common methods for overcoming signal attenuation are to either abrasively remove the outer layers of the skin and apply conducting electrolytic gels, or enter the body invasively through needle electrodes. However, neither of these methods is desirable: removal of skin can be painful and time consuming; the use of conductive gels is not only uncomfortable and inconvenient but also unsuitable for long-term recordings, as the gel tends to evaporate [8] and causes inflammation and swelling in some cases [9–11]. Invasively entering the body using needle electrodes causes undesirable discomfort to the patient and hence is not a suitable technique for diagnostics. A couple of alternatives for these so-called wet electrodes have been reported—an active electrode strategy by Alizadeh-Taheri *et al* and Nishimura *et al* [12, 13] where a dry silicon electrode chip and a CMOS chip are packaged together to record and process the signal simultaneously. Although the idea of having electronics to amplify and process signals in close proximity to bioelectrodes is novel in its scope, this approach still ignores the fact that the electrode technology is practically unchanged for standard wet electrodes. Additionally the integration process used to connect the electrode and CMOS chips is complex and not repeatable. The nature of these measurements makes disposing the electrodes after one time use a key characteristic (due to personal health and hygiene). The other strategy is a class of dry spiked electrodes, reported by Griss *et al* [6, 14], Lin *et al* [8] and Sullivan *et al* [15]. The dry spiked electrodes circumvent the skin impedance problem by using microfabricated 3D silicon electrodes to painlessly pierce the SC, providing direct access to the more conductive stratum granulosum (SG). The comparison between dry spiked and wet electrodes is depicted schematically in figure 2. These dry spiked electrodes have the additional advantage of significantly reducing the electrode footprint without increasing the electrode impedance [8]. A reduced electrode area enables much greater specificity, including more targeted and effective stimuli and higher spatial resolution recordings. Despite the benefits reported in these dry spiked electrode strategies, they suffer from two significant drawbacks: (1) expensive, multilayer cleanroom processing, and (2) material limitations (silicon-based technologies with no other material set). These technologies involve multi-step silicon dry and wet etching followed by single or multiple metal deposition steps to define the electrodes. These processes are compatible only with silicon micromachining and cannot be adapted to materials like biocompatible polymers. The expense and material limitations imposed by this technology greatly diminish its prospect for commercial viability, making it unlikely for researchers and clinicians to ever reap its benefits. Therefore, a technology

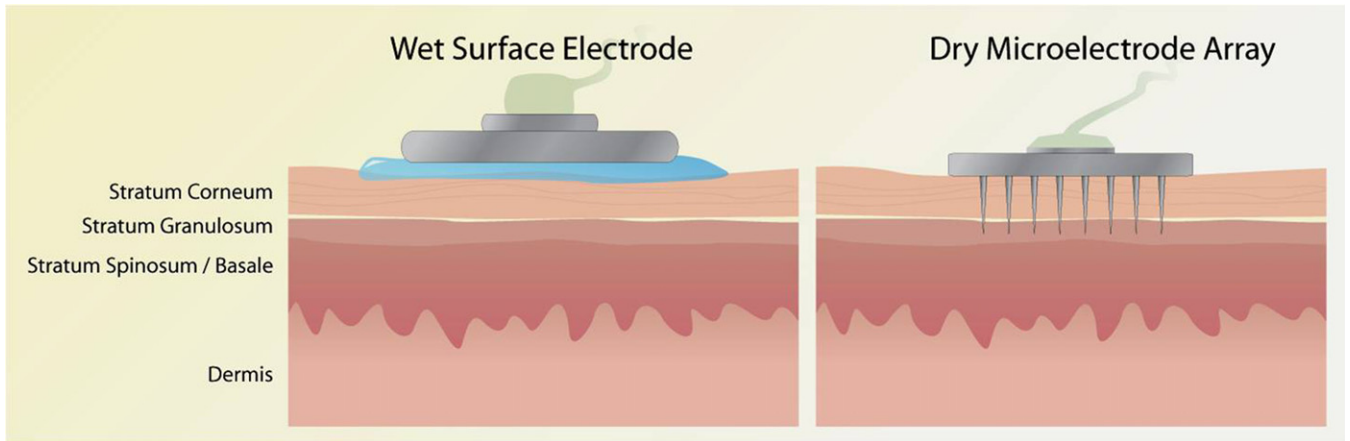


Figure 2. Comparison between wet and dry biopotential electrodes: (left) wet electrodes that sit on the surface of the skin and need preparation like the use of electrolytic gel (shown here). Dry micromachined electrodes (right) do not require extensive preparation since they pierce the outer layers of the skin and achieve a low impedance pathway to recording neural signals.

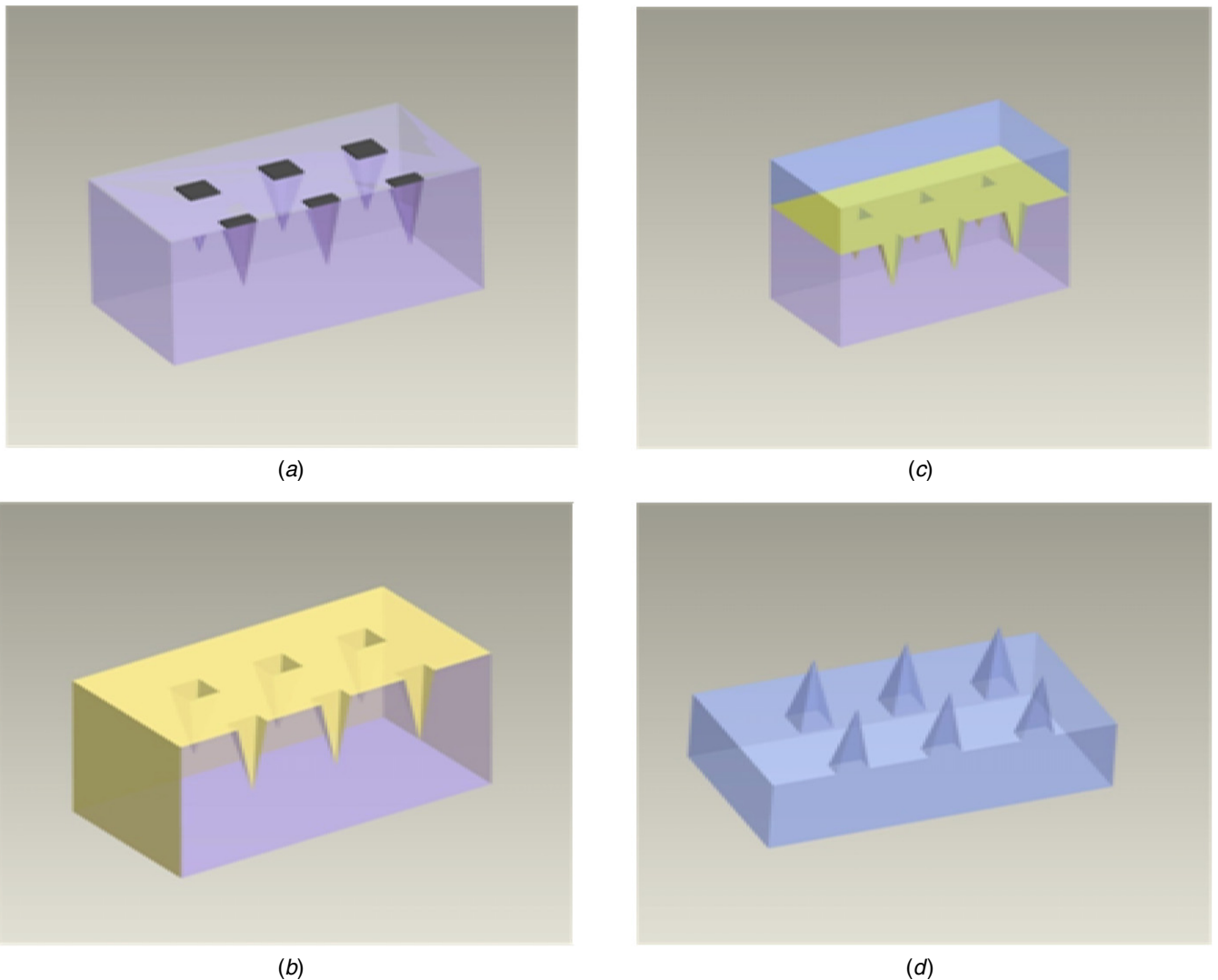


Figure 3. Fabrication process flow for master structure fabrication using inclined UV exposure of SU-8: (a) inclined UV exposure of SU-8 to define trenches; (b) develop the uncrosslinked SU-8 away and metalize the rigid mold; (c) cast PDMS in the rigid mold; and (d) demold PDMS master from the rigid mold.

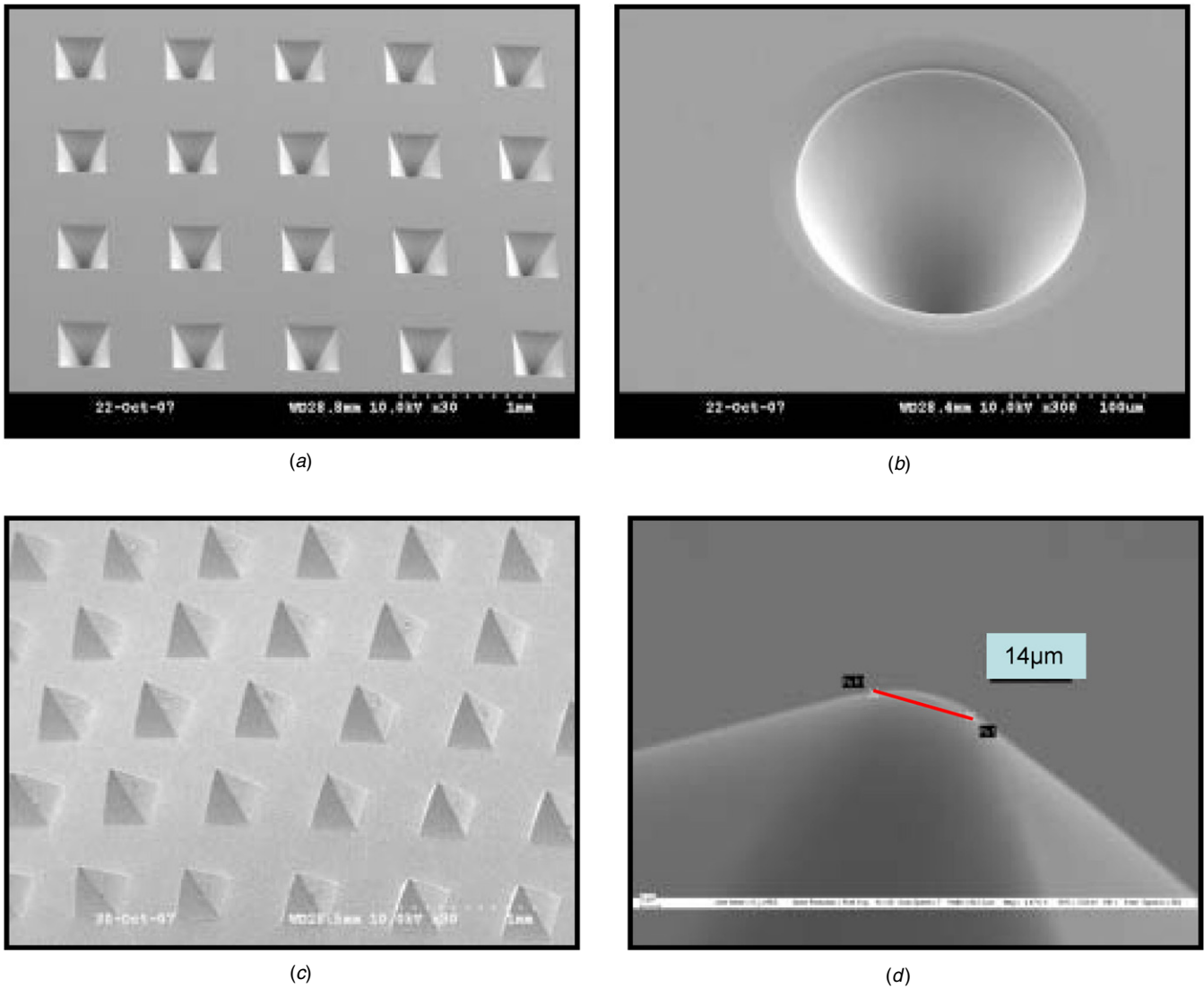


Figure 4. SEM images of (a) pyramidal SU-8 rigid mold; (b) conical SU-8 rigid mold; (c) pyramidal PDMS master array; and (d) closer view of the tip of the needle depicting the level of sharpness (hard to control and non-uniform across a single array).

that combines 3D functionality, scalability, and cost-effective micro-manufacturability is required to provide pain-free, high-fidelity electrodes that overcome the skin impedance problem.

Metal transfer micromolding (MTM) is introduced in this paper as a potential candidate for achieving such biopotential 3D MEAs with controllable electrode height and electrode tip sharpness to suit the intended application. MTM has several distinct advantages which can be exploited to overcome the above listed manufacturing, materials and skin impedance challenges: (a) a simultaneous metalization scheme that allows for micromolding and metalization of microneedles in a single step; (b) a micromolding-based approach which lends itself to scaling and mass manufacturing; (c) process control to achieve the desired tip sharpness of the microelectrode array; and (d) a material set consisting of biocompatible polymers. The design chosen for the 3D MEA (as seen in the schematic in figure 1) is a 5×5 array of metalized towers in the center of the chip. The electrodes are accessed from the backside of the array. The overall chip dimensions are $5 \text{ mm} \times 5 \text{ mm}$ with the base

of the towers being $250 \mu\text{m}$. The pitch between the micro-towers can be varied according to the required application. The height of the towers is designed to be around $300 \mu\text{m}$ for the penetration of the SC layer. The sharpness of the tips of the micro-towers can be controlled and is usually lower than $20 \mu\text{m}$, which is sufficient for making contact with the SG layer [16]. The fabrication and packaging of such a device is reported in this paper. Impedance spectrum measurements and a nerve tracking demonstration utilizing these MTM 3D MEAs are further explored in this work.

2. Microfabrication and packaging

2.1. Master structure fabrication: inclined UV lithography

The negative-tone resist SU-8 is used to fabricate a wide variety of MEMS structures like mechanical structures [17], microfluidic devices [18], high-aspect-ratio structures [19] and rigid molds [20] due to its chemical inertness, ease of photo definition and capability for single layer high-aspect-ratio

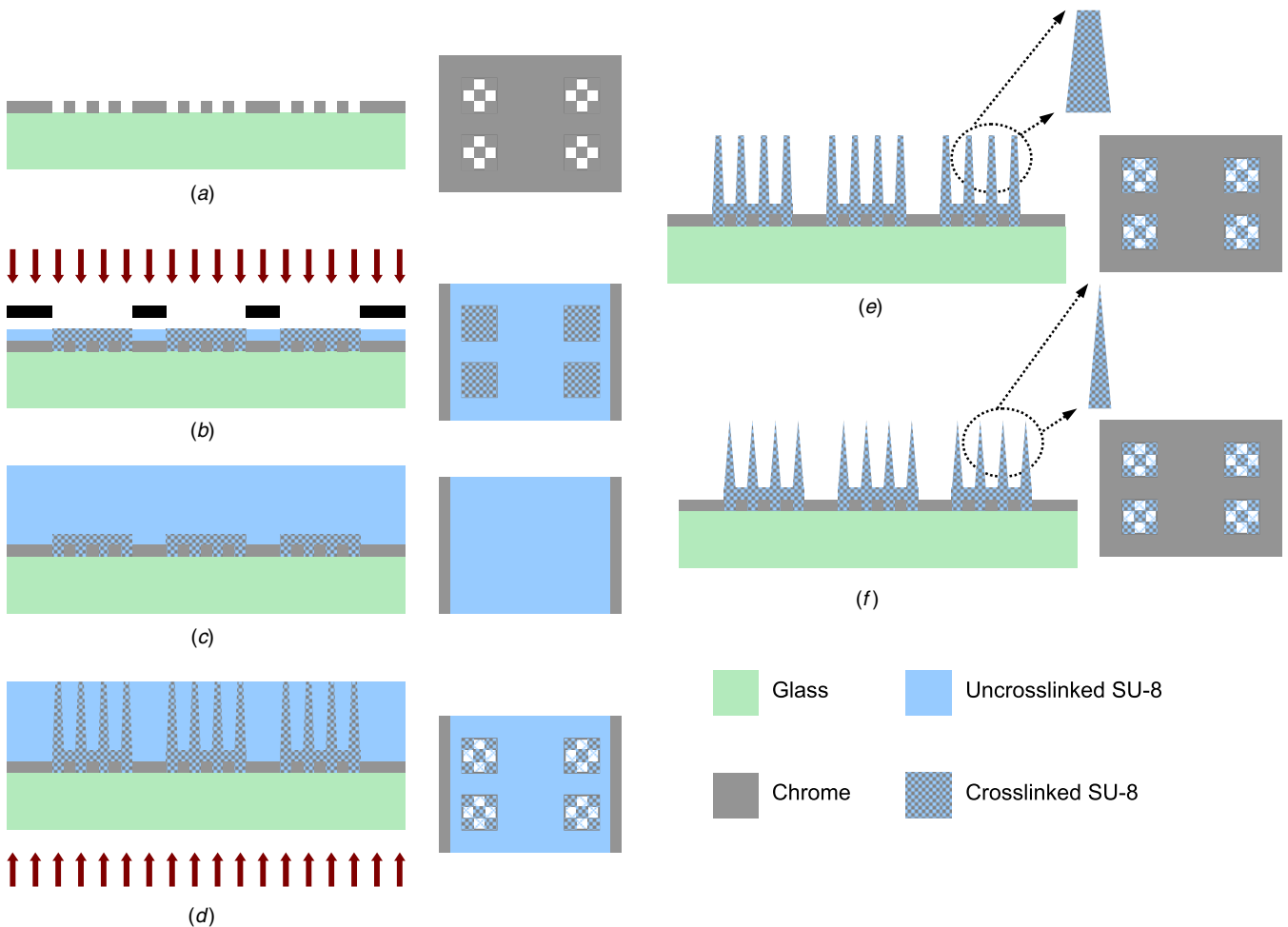


Figure 5. Process flow for master structure fabrication using double-side exposure of thick SU-8. The schematic on the left-hand side depicts the side view of the process steps and the one on the right-hand side depicts the top view of the steps: (a) definition of the micro-tower positions on a chrome plate; (b) top side exposure of thin SU-8 to define the base substrate for the master; (c) coating thick SU-8 without developing the thin SU-8 layer; (d) controlled backside exposure of thick SU-8 to define taper shaped tower arrays; (e) develop both layers of SU-8 simultaneously; and (f) sharpen the master structure using the RIE.

microfabrication. Most of these reported applications utilize standard top side UV lithography of single layer or multilayer SU-8. We have developed inclined rotational UV lithography of SU-8 to microfabricate complex 3D structures [21, 22]. The dimension of the masking feature and angle of inclination control the shape and depth of the created trench in SU-8. The process flow for master structure fabrication using inclined UV lithography is schematically illustrated in figure 3. The first step in this process is the casting of thick SU-8 ($\sim 700 \mu\text{m}$) on a silicon substrate and the definition of a 5×5 MEA array trench footprint on it using the inclined rotational exposure process (figure 3(a)). A release layer of Cr/Au (10 nm/150 nm) is coated on the SU-8 trenches using a sputtering system (figure 3(b)). Pre-mixed polydimethylsiloxane (PDMS) is cast in these trenches (figure 3(c)) and cured. The PDMS structure is demolded to release the master (figure 3(d)). Figures 4(a) and (b) portray the SEM images of a conical and pyramidal SU-8 mold, respectively. Figures 4(c) and (d) depict the SEM images of the PDMS master. 3D MEAs are micromolded from this master structure (section 2.3).

2.2. Master structure fabrication: thick SU-8 exposure and RIE etching

One of the issues with the inclined UV exposure of SU-8 is that the sharpness at the tip of the constructed micro-tower is non-uniform across a single array and difficult to control. The PDMS master structure can be optionally sharpened but sharpening of PDMS requires anisotropic dry or wet etching which is not easily accomplished [23]. Even though some success has been reported in anisotropic etching of PDMS by Garra *et al*, surface roughness and non-uniformity are reported as problems that require further development. Hence, we explored alternative techniques/materials which will allow for the fabrication of master structures where the geometry of the tip can be tuned. Controlled backside exposure of thick SU-8 followed by RIE sharpening can yield the tuning required for an application such as the one reported in this work. This master structure is constructed on an SU-8 substrate. The fabrication process flow for such a technique is shown in figure 5. The process begins with the definition of the locations of the micro-tower arrays on a 4" chrome mask (figure 5(a)). The micro-tower locations are transferred to

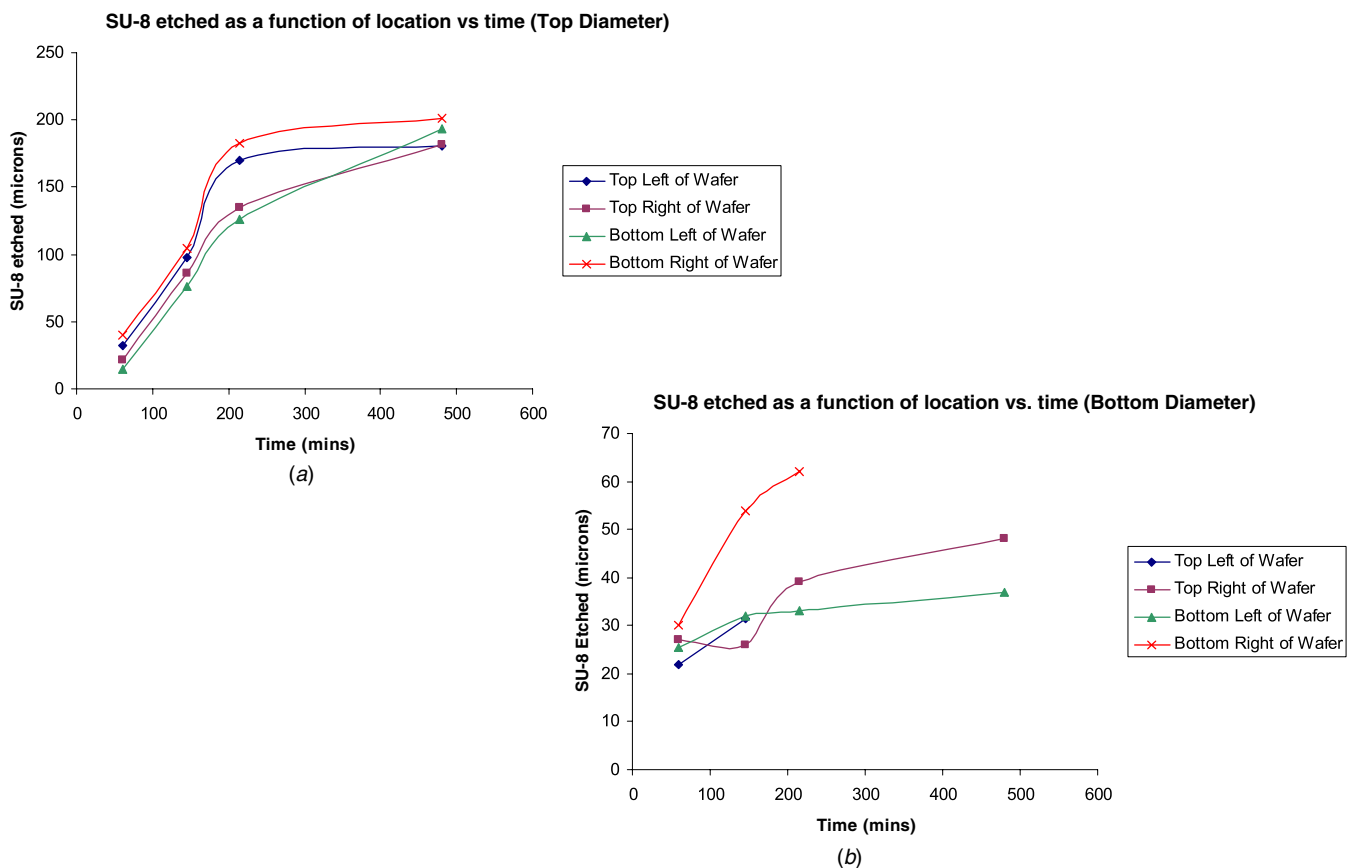


Figure 6. Anisotropic etching of SU-8 in the RIE: (a) top diameter of the micro-towers as a function of location on the substrate and time; and (b) bottom diameter of the micro-towers as a function of location on the substrate and time.

the chrome plate using a high resolution transparency that is designed in AutoCAD and printed by a commercial high resolution mask manufacturer (Fineline Imaging, Colorado Springs, CO). A ‘thin’ layer of SU-8 ($\sim 100 \mu\text{m}$) that will serve as the substrate for the final structures is spin coated and baked according to the manufacturer’s datasheet (Microchem Inc., Newton MA). A second mask with square patterns that will serve as the device substrate for the final micro-towers is used to expose the ‘thin’ layer of SU-8 using traditional top side lithography (figure 5(b)). A second layer of SU-8 (‘thick’ SU-8) is coated (after a post-exposure bake but without developing the first layer) and soft baked at 95°C for 24 h (figure 5(c)). The thickness of this layer defines the height of the final MEAs and is $300 \mu\text{m}$, in order to successfully penetrate the SC layer. This layer is exposed from the backside using a larger dose to accommodate the thicker SU-8 (figure 5(d)). The exposure parameters are controlled to achieve a taper shape (as shown in the inset of figure 5(e)), such that the towers can be sharpened. Both the layers are simultaneously developed using PGMEA (Microchem Inc., Newton, MA) with stirring after a post-exposure bake of 1.5 h at 95°C (figure 5(e)). In order to fully crosslink the epoxy a blanket exposure is performed after the development process. The structures are etched (figure 5(f)) in a Plasma Therm RIE system (Plasma Therm Inc., St Petersburg, FL) to sharpen the master structure using a 10:1 gas mixture of O_2 and CHF_3 , respectively. A power level of 100 W and a pressure of

1000 mT were used in this recipe. These parameters were chosen to achieve an anisotropic etch rate of SU-8 that etches the top of the micro-towers (top diameter; initial average value: $220 \mu\text{m}$) faster than the base of the towers (bottom diameter; initial average value: $260 \mu\text{m}$). The amount of SU-8 etched was measured as a function of time and location on the 4" substrate to ascertain the tip sharpness as well as to monitor the etch rate variation across a 4" substrate. This value is plotted as a function of time and is shown in figure 6(a) for the top diameter and figure 6(b) for the bottom diameter. Although the required anisotropy (greater than 3:1) and hence sharp tips (radius $\sim 10\text{--}15 \mu\text{m}$) are achieved in this process, a variation in the amount of SU-8 etched as a function of micro-tower location is consistently present. The lack of control of materials used in the RIE tool and the age of the tool are the most likely reasons for this variation. Figures 7(a)–(d) depict the optical micrographs of various micro-tower array master structures fabricated using this process.

2.3. Fabrication of 3D MEAs from the master structure: MTM

The fabrication of the final 3D MEAs from the master structure involves two molding steps: first to construct a flexible mold that has the same shape as the rigid SU-8 mold fabricated in section 2.1 and the second to fabricate the MEAs from this flexible mold. Once the master structure has been fabricated

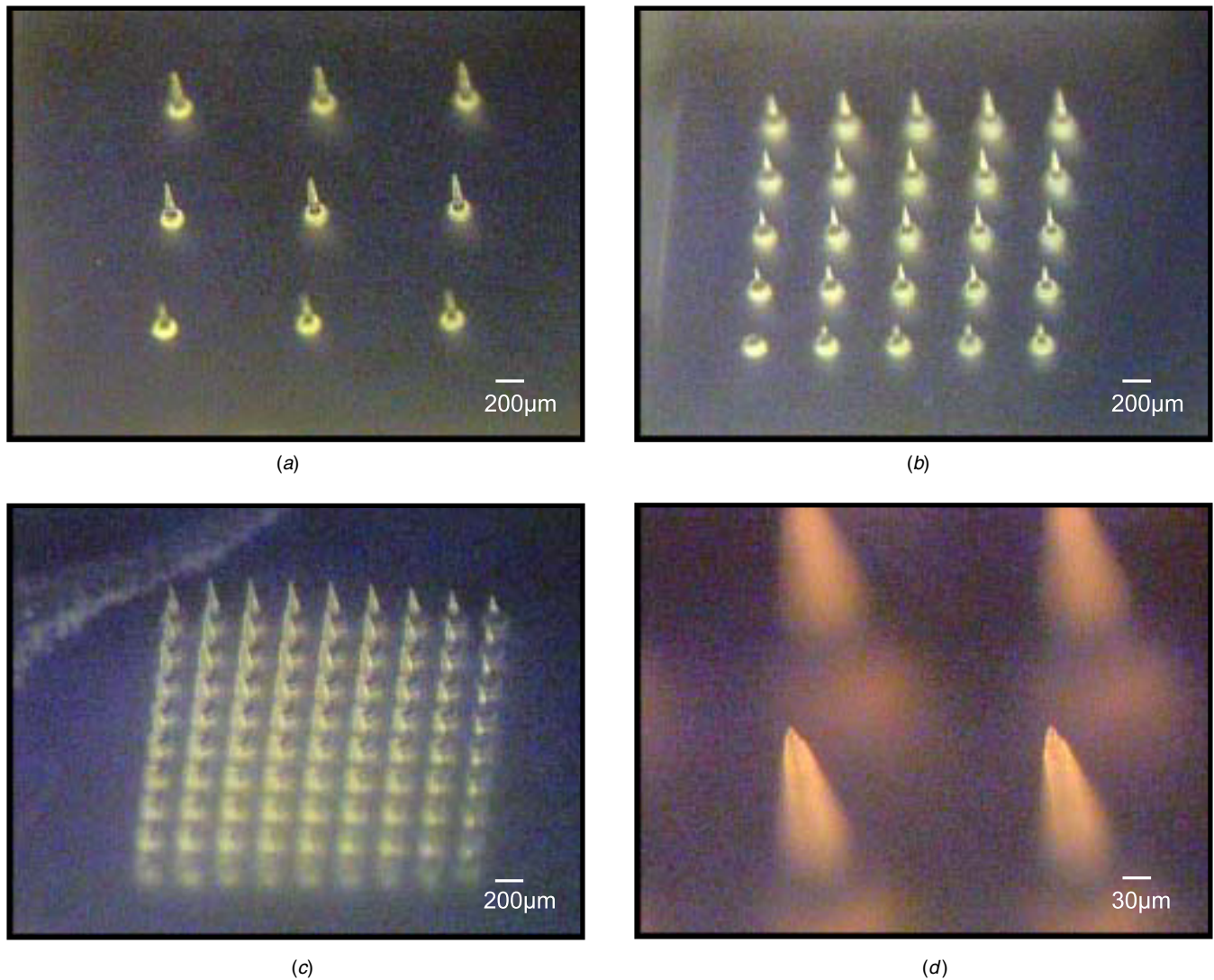


Figure 7. Optical micrographs of master structures fabricated using the double-side exposure of thick SU-8 followed by RIE etching: (a) 3×3 array of sharpened micro-towers; (b) 5×5 array of sharpened micro-towers; (c) 9×9 array of sharpened micro-towers; and (d) close-up view of the micro-towers depicting the level of sharpness.

(using either of the two techniques described above), it can be used multiple times to yield 3D MEAs using these two steps. This two-step molding process is depicted in figure 8. It begins with the coating of a release layer, Cr/Au (10 nm/150 nm) on the SU-8 or PDMS master (figure 8(a)). The PDMS is cast onto this structure (figure 8(b)). Once the PDMS is cured into a flexible mold, it is demolded from the rigid master (figure 8(c)). A functional metal layer is embedded in the final 3D MEAs by coating a layer of Au/Cr (300 nm/15 nm) using a sputter coater (figure 8(d)) on the flexible mold (relatively low temperature deposition compatible with polymer processing) and transferring it to the final structure (made out of polymethylmethacrylate: PMMA) during the molding process (figure 8(e)). This is accomplished due to the surface energy differences between PDMS and PMMA [24, 25]. A process of solvent casting is used in this final molding process. 3D MEAs with functional metal layers are demolded from the PDMS mold thereby ensuring lower processing steps (figure 8(f)). The chrome layer deposited

on the mold acts as an adhesion promoter for the functional gold electrode layer and also helps to improve uniformity. The transfer of metal from PDMS to PMMA is very reproducible and has been performed in over a hundred devices. Further, the adhesion of the metal to the substrate using the MTM process has been shown to be comparable to directly deposited films on polymers [26]. Figure 9 illustrates the optical micrographs and SEM images of 3D MEAs constructed using the MTM process. The device in figure 9(a) is made from a master structure fabricated using the inclined UV lithography technique. The devices depicted in figures 9(b) and (c) are fabricated from a master structure produced using the techniques described in section 2.2.

2.4. Packaging of 3D MEAs

The packaging process for the biopotential MEAs needs to be simple and inexpensive as these devices are intended for hygienic single use. The backside of the 3D MEAs was

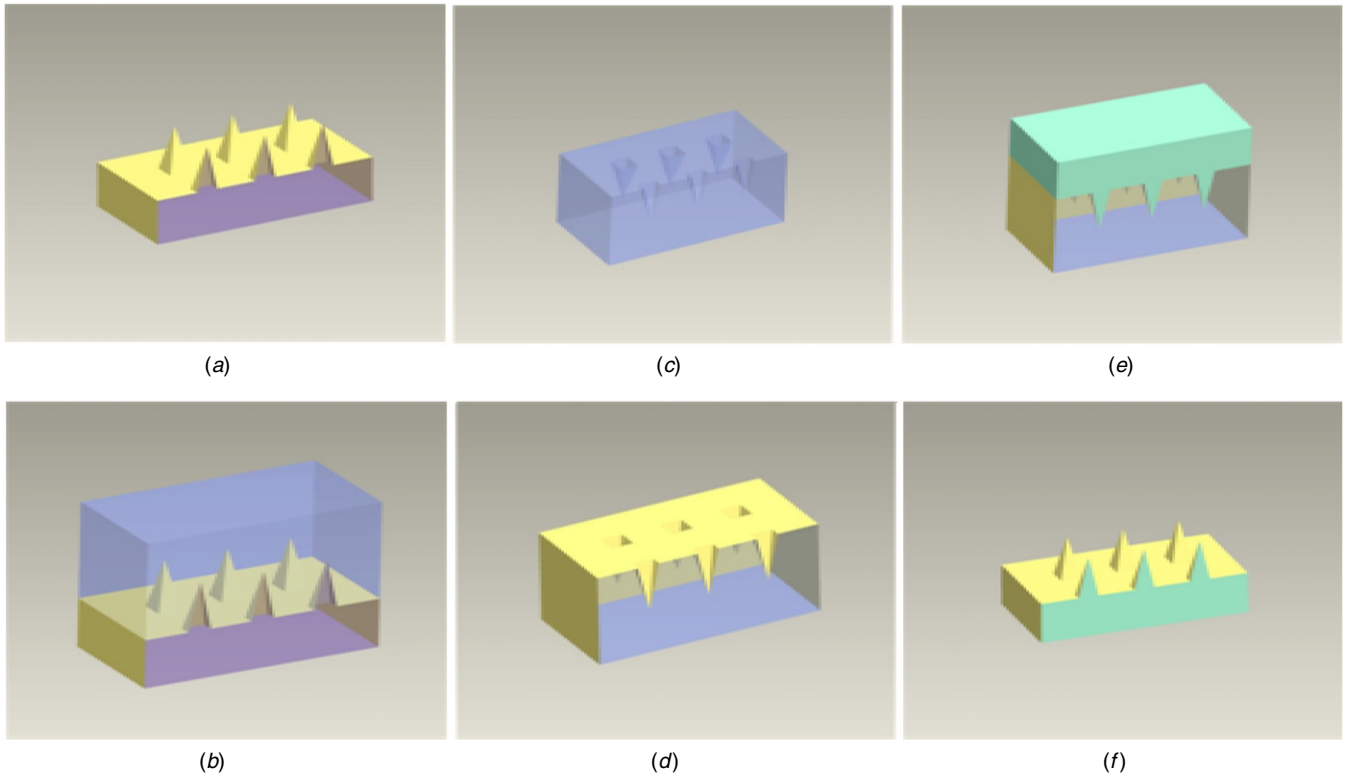


Figure 8. Fabrication process flow for 3D MEAs from master structures: (a) metalize the master structure; (b) cast PDMS on metalized master to fabricate the flexible mold; (c) demold flexible mold from the master structure; (d) metalize flexible mold; (e) cast PMMA on metalized PDMS mold; and (f) demold functional 3D MEAs with functional metal layers.

metalized to achieve front to back electrical continuity. This was performed on a sputter coater with a 15 nm/200 nm layer of chromium/gold. A Kapton® sheet (~125 μm thick) was machined into 16 mm circular substrates with a 5 mm central port using a CO₂ laser (LS-500 New Hermes-Gravograph, Duluth, GA). The 3D MEA was attached to this substrate utilizing a layer of two-part epoxy. For backside interconnection, a wire was attached to the MEA using conductive epoxy (Master Bond, Hackensack, NJ). The front–back electrical connectivity is confirmed using a multimeter.

3. Testing and results

The microfabricated and packaged MTM MEAs (made out of the polymer PMMA) are characterized utilizing minimally invasive *in vivo* biopotential measurements. A NCS demonstration was selected as the appropriate vehicle for *in vivo* MEA characterization since, for a given electrode area, improvements in NCS measurements over those achievable using conventional electrodes, that do not pierce the SC, would demonstrate the reduced impedance principle of the 3D MEAs. In addition, the impedance spectrum of these devices was measured and compared to standard wet electrodes. These *in vivo* experiments involved human subjects and were performed with the approval of Institutional Review Board (IRB) of Emory University (Atlanta, GA). The mechanical characterization of such devices has been demonstrated to be

adequate for a microneedle application [27] and hence has not been performed as part of this work.

3.1. Electrode–skin–electrode impedance measurements

The primary metric for evaluating electrode performance was the full spectrum measurement of the electrode impedance magnitude. In order to facilitate such measurements, a custom setup was developed. A desktop computer, via a custom MATLAB interface, coordinated all communication between a dynamic signal analyzer (Stanford Research SR725, through GPIB) and the custom switching board (PIC 18F442, through RS-232). For full spectrum impedance measurements, the signal analyzer was configured to source a small (60 mV), sweeping, sinusoidal voltage. For evaluating the performance of the electrodes, the automated switching and measuring system was configured to apply this voltage across two skin-surface electrodes placed on the forearm of a test human subject and a reference resistor, as shown in the circuit represented in figure 10(a). Specifically, the spectrum analyzer measured the voltage across the electrode pair and a 100 kΩ reference resistor using two instrumentation amplifiers (INA129P). MATLAB software was used to calculate the impedance magnitude according to the equation

$$Z_{\text{ELECTRODE}} = R_{\text{REF}}(V_{\text{ELECTRODE}}/V_{\text{REF}}). \quad (1)$$

The characterization was first performed with standard commercial wet electrodes (Meditrace Biopotential

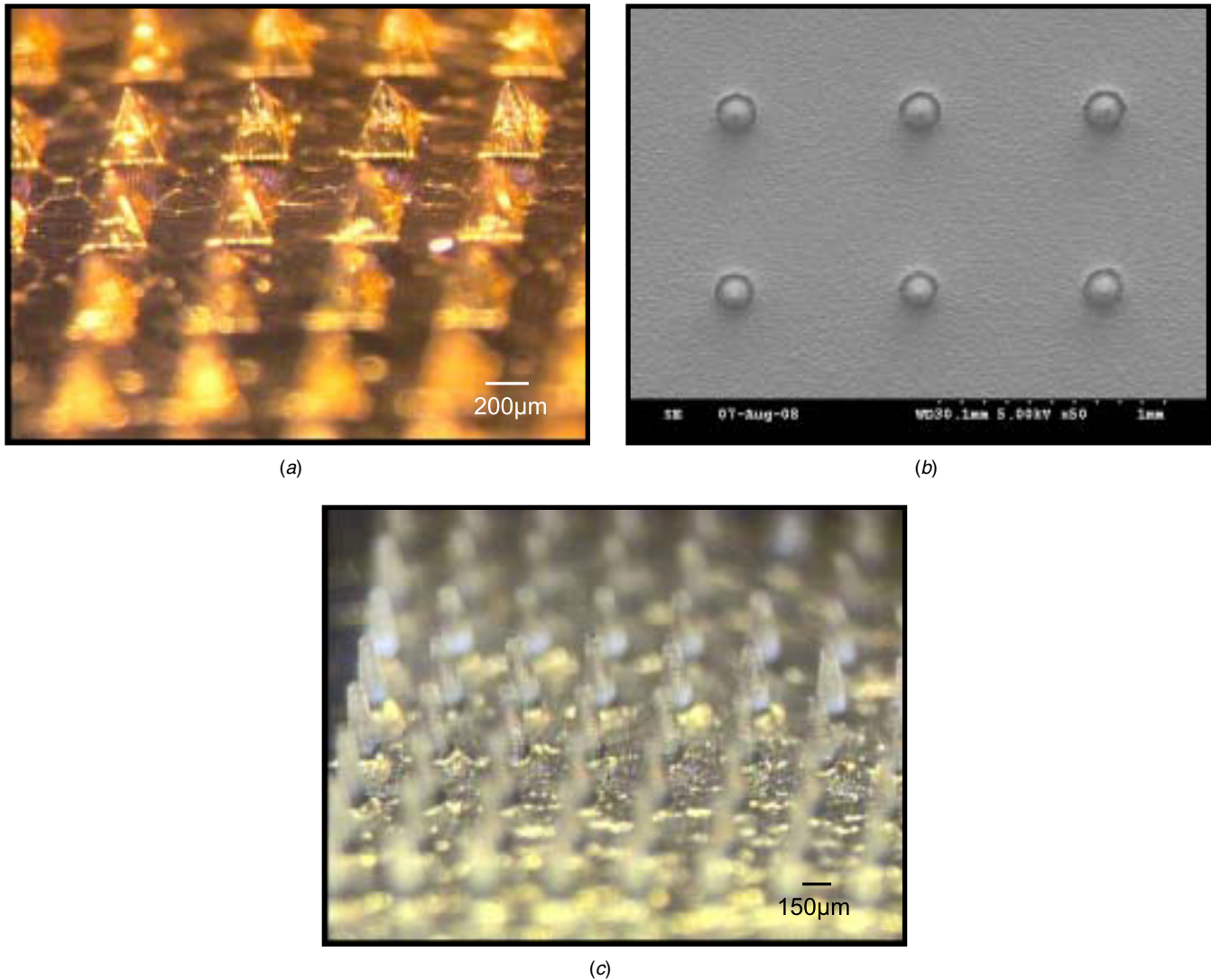


Figure 9. SEM and optical micrographs of 3D MEAs: (a) 9×9 array fabricated utilizing inclined UV lithography master; (b) 5×5 array fabricated using a master structure made from double-side exposure/RIE etching of thick SU-8; and (c) 9×9 array fabricated using a master structure made from double-side exposure/RIE etching of thick SU-8.

electrodes, Rochester Electro-Medical Inc., Tampa, FL) and then repeated with the 3D MEAs. Multiple sets of measurements were taken using this protocol. The 3D MEAs were held in place on the test subject's forearm with medical tape. Figure 10(b) shows frequency spectrum plots of the impedance of commercial and 3D electrodes for one such representative measurement. The impedance is normalized to the area of the electrodes (area of commercial electrodes: 314.159 mm^2 , area of 3D MEAs: 25 mm^2 . This calculation is performed using the stated areas of the two types of electrodes. In fact, the area of the wet electrodes would be higher due to gel perfusion into the skin and the MTM 3D MEAs would have a lower area accounting for the protruding tips alone but these effects are neglected in order to simplify the calculation) and is an order of magnitude lower for 3D MEAs. The importance of the lower impedance of the 3D MEAs is paramount in nerve tracking and disease monitoring applications, where an array of individually addressable electrodes is required in a patch-like format to improve

the resolution of the measurement. The 3D MEAs can be extended to such high-density arrays due to their smaller footprint to achieve better spatial resolution and higher fidelity signals compared to standard wet electrodes.

3.2. EMG measurements

EMG is the study of the muscle function through the measurement of the electrical signals that emanate from muscles. The signal itself is an electrical manifestation of the neuromuscular activity associated with a contracting muscle [28]. It is a complicated signal that depends on several factors, including the properties of the muscle that is contracting, the control scheme of the peripheral nervous system and the instrumentation that is being used to measure it. The measurement of this signal has several applications in a clinical diagnosis setting—sensing fatigue in muscle during strengthening and conditioning [29]; monitoring facial EMG measurements to study early indications of stroke and paralysis

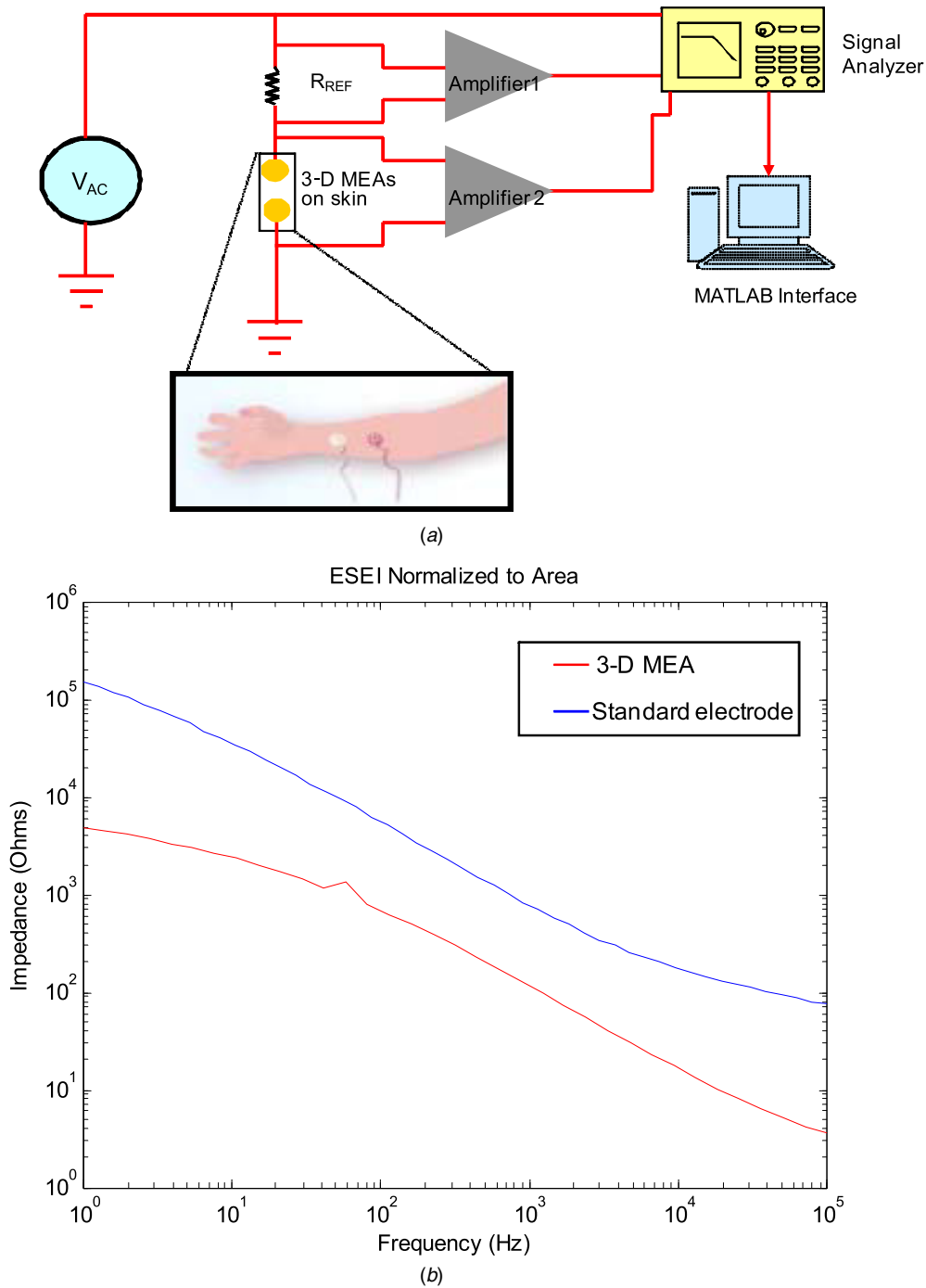


Figure 10. Electrode impedance measurement on a skin interface: (a) measurement circuitry; (b) representative full frequency spectrum electrode measurement for both wet standard electrodes and 3D MEAs. The measurements have been normalized to the area to accommodate the differences in the areas of standard wet electrodes and 3D MEAs.

[30]; characterizing disease or dysfunction, such as carpal tunnel syndrome [31]. The measurement of EMG using 3D MEAs demonstrates the applicability of these devices to a variety of clinical studies even though these studies are outside the scope of this paper. The setup developed to measure EMG signals is depicted in figure 11(a) and consists of two recording electrodes and a reference electrode (which is placed further away from the recording electrodes, so as to have no influence on the muscular signal of interest). These recording electrodes detect two potentials in the muscle of interest (in our case

forearm). These two signals are then fed to a differential amplifier which amplifies the difference of the two signals, thus eliminating any common mode components in the two signals. The differential amplifier used in this measurement is a Brownlee 440 amplifier setup (Tektronix Inc., Richardson, TX). The gain used is 2 K with a bandwidth of 75–500 Hz. The raw analog signal is then converted into a digital signal by a D-Space A/D converter (dSPACE GmbH, Paderborn, Germany) and subsequently read out by an oscilloscope or a computer (for the MATLAB interface).

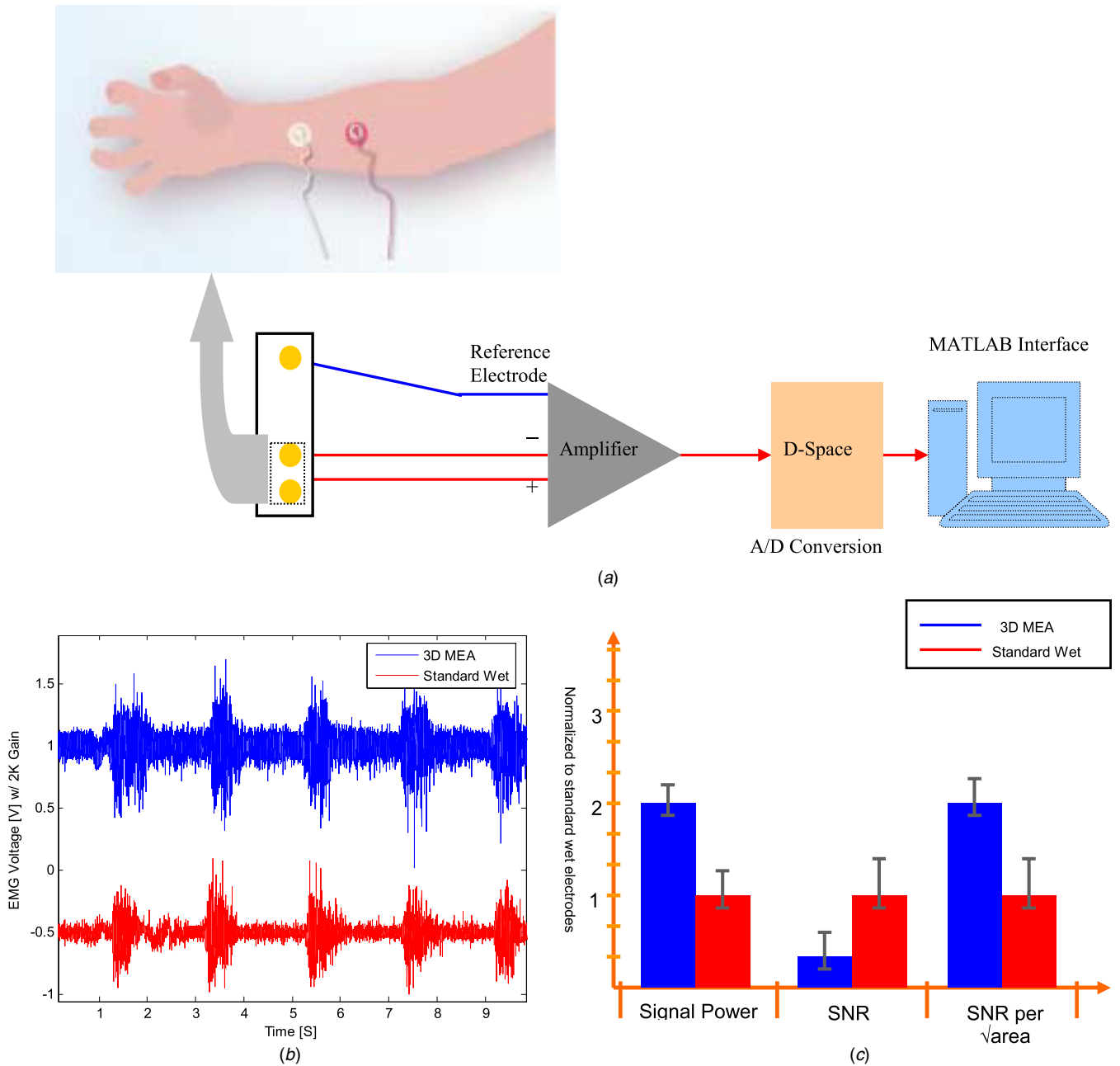


Figure 11. EMG test setup and results: (a) measurement setup; (b) example of a raw EMG signal procured from standard wet electrodes and 3D MEAs; (c) extraction of signal power, SNR and SNR/ $\sqrt{\text{area}}$ for all the experiments with error bars. Note that these data have been normalized to standard electrode values to provide a simple comparison.

Figure 11(b) depicts raw EMG data collected from standard wet recording electrodes and 3D MEAs. Figure 11(c) provides an analysis of the results for multiple sets of experiments on the same human test subject. This analysis consistently demonstrates a 100% improvement in signal power for the 3D MEA recording electrodes, as compared to the wet recording electrodes, even though the noise signal is marginally higher for the MEAs. The ratio of the electrode area between the wet and dry electrodes is 12.56:1 and noise in EMG measurement is predicted to scale with $1/\sqrt{\text{area}}$ of the electrodes [32], justifying the noise characterization.

3.3. Nerve conduction measurements

Electrodes for bioelectric signal measurement demonstrate their fullest potential when they can be reliably used for *automated* diagnostic, prosthetic, and therapeutic applications. Unfortunately, person-to-person anatomic variability coupled with bioelectrode signal loss (i.e. the skin impedance problem) and signal distortion greatly hinders automation. As a result, many biopotential applications require the manual attention of highly skilled operators. This is especially true in the context of NCS, which are used to diagnose disorders of peripheral nerve and muscle ranging from carpal tunnel syndrome to amyotrophic lateral sclerosis (ALS—Lou Gehrig’s disease).

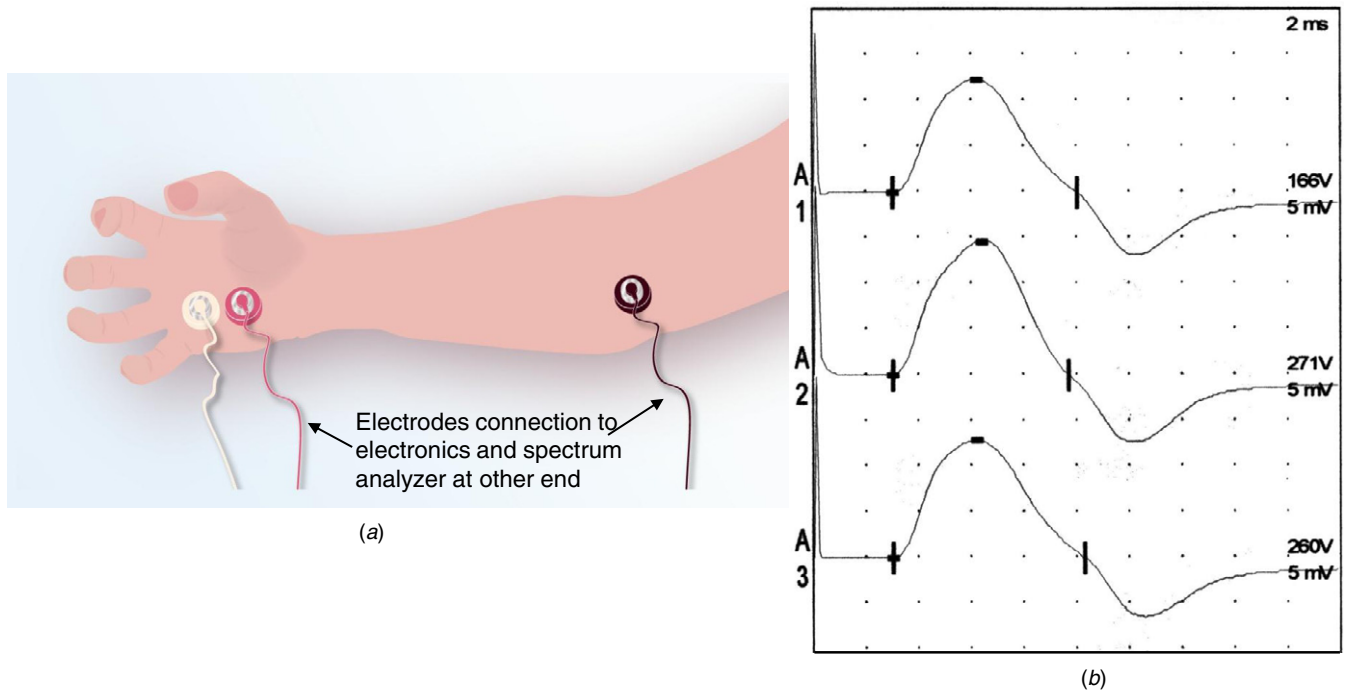


Figure 12. (a) Electrode placement for NCS; and (b) representative nerve conduction measurements on test subject: (A1) with standard wet electrodes; (A2) with 3D MEAs showing better amplitude and sharper rise times as compared to A1 (voltage values on the right-hand side); and (A3) with standard electrodes after using 3D MEA which shows improved performance.

The demonstration of NCS in this work was carried out using an FDA-approved Nicolet Viking IV EMG unit (Nicolet Biomedical, Madison, WI). Recording electrodes were placed over the abductor pollicis brevis muscle of the left hand of a test human subject with the active electrode over the belly of the muscle, a reference electrode over the proximal knuckle and a ground electrode over the dorsum of the hand as shown in figure 12(a). Voltage stimuli (duration 100 ms) were applied over the median nerve at the wrist; the stimulus intensity was started at 50 V and gradually increased until a supramaximal response amplitude was obtained. In all experiments, the supramaximal response amplitude was achieved at voltages less than the maximum stimulus voltage of 400 V. The response amplitude was measured as the maximum negative deviation of the recorded waveform from baseline. Distal latency was measured as the delay between the delivery of the stimulus and the initial deviation of the response from the baseline.

Figure 12(b) shows a representative graph of the results for the motor NCS performed on the median nerve of a single subject. This figure compares the evoked compound motor action potential recorded by conventional wet electrodes (trace A1) and 3D MEA (trace A2) for one such representative measurement. The measurements using the 3D MEAs were performed an hour after the measurement with the wet electrodes in order to minimize the influence of the conducting gel on the 3D MEA trace. The response recorded by the 3D MEA showed larger amplitude and a faster rise time, suggesting lower electrode impedance in all measurements. Recordings using conventional electrodes post-MEA measurements (immediately performed; trace A3) show improved characteristics, suggesting piercing of the SC layer by the MTM 3D MEAs.

4. Discussion and conclusions

Minimally invasive biopotential electrodes have an enormous scope in neural therapeutics, prosthetics and clinical diagnostics. The standard electrodes used in these applications are surface and *wet* electrodes that require extensive preparation of the skin to circumvent the high impedance of the outer layers, in order to precisely sense low-amplitude biopotentials. We have demonstrated a *dry* approach where, with the aid of 3D MEAs, the skin impedance problem is eliminated and the preparation required for measurements is drastically reduced. These 3D MEAs are fabricated utilizing metal transfer micromolding technology, which has the potential to fabricate 3D MEAs relatively easily, and potentially mass manufacture them in a cost-effective fashion. Two non-traditional microfabrication technologies: an inclined UV lithography and double-sided exposure of thick negative resist, followed by RIE sharpening, have been demonstrated for the 3D MEA master structure fabrication. The MEAs themselves are micromolded from the master structure and a functional metal layer is embedded in them during this step. These MEAs have been packaged using biocompatible Kapton[®] substrates. In order to demonstrate biopotential measurements a nerve tracking demonstration is carried out with electromyography and nerve conduction performed on test human subjects. The EMG measurements show a 100% increase in both signal power and SNR/ $\sqrt{\text{area}}$ as compared to standard wet electrodes. Nerve conduction measurements that show faster rise times and larger amplitude signals as compared to standard electrodes have been demonstrated. The most important parameter for biopotential electrodes is electrode–skin–electrode impedance

(ESEI) measurement. ESEI measurements show an order of magnitude improved performance for impedance of the 3D MEAs as compared to standard electrodes (normalized to the area of each). Solutions to several clinical diagnostic tools are dependent on the ability to precisely sense and manipulate the human nervous system and biopotential electrodes are one of the key components along with data processing chips and software that serve to transduce biopotentials. We believe that the technologies demonstrated in this work represent a non-traditional approach to biopotential electrodes that will improve the resolution and information content of present-day clinical neurologic diagnostics.

Acknowledgments

The authors would like to thank Mr Brock Wester for his assistance with the MEA schematics and 3D figures. The microfabrication of the MEAs was performed at the Georgia Tech Microelectronics Research Center cleanroom facility.

References

- [1] Wise K D 2005 Silicon microsystems for neuroscience and neural prostheses *IEEE Eng. Med. Biol. Mag.* **24** 22–9
- [2] Scherder E, Bouma A and Steen A 1996 Effects of a follow-up treatment of short-term transcutaneous electrical nerve stimulation on memory and affective behaviour in a patient with probable Alzheimer's disease *Behav. Neurol.* **9** 33–5
- [3] Farina S, Granella F, Malferrari G and Manzoni G C 1986 Headache and cervical spine disorders: classification and treatment with transcutaneous electrical nerve stimulation *Headache* **26** 431–3
- [4] Disselhorst-Klug C, Bahm J, Ramaekers V, Trachterna A and Rau G 2000 Non-invasive approach of motor unit recording during muscle contractions in humans *Eur. J. Appl. Physiol.* **83** 144–50
- [5] De Luca C J 2006 Electromyography *Encyclopedia of Medical Devices and Instrumentation* (New York: Wiley)
- [6] Griss P, Enoksson P, Tolvanen-Laakso H K, Merilainen P, Ollmar S and Stemme G 2001 Micromachined electrodes for biopotential measurements *J. Microelectromech. Syst.* **10** 10–6
- [7] Miller H A and Harrison D C 1974 *Biomedical Electrode Technology: Theory and Practice* (New York: Academic)
- [8] Lin C T, Ko L W, Chiou J C, Duann J R, Huang R S, Liang S F, Chiu T W and Jung T P 2008 Noninvasive neural prostheses using mobile and wireless EEG *Proc. IEEE* **96** 1167–83
- [9] Searle A and Kirkup L 2000 A direct comparison of wet, dry and insulating bioelectric recording electrodes *Phys. Meas.* **21** 271–83
- [10] Dwyer C M, Chapman R S and Forsyth A 1994 Allergic contact-dermatitis from TENS gel *Contact Dermat.* **30** 305
- [11] Uter W and Schwanitz H J 1996 Contact dermatitis from propylene glycol in ECG electrode gel *Contact Dermat.* **34** 230–1
- [12] Alizadeh-Taheri B, Smith R L and Knight R T 1995 An active, microfabricated, scalp electrode-array for EEG recording *Transducers '95: 8th Int. Conf. on Solid-State Sensors and Actuators, 1995 and Eurosensors IX* pp 67–70
- [13] Nishimura S, Tomita Y and Horiuchi T 1992 Clinical application of an active electrode using an operational amplifier *IEEE Trans. Biomed. Eng.* **39** 1096–9
- [14] Griss P, Tolvanen-Laakso H K, Merilainen P and Stemme G 2002 Characterization of micromachined spiked biopotential electrodes *IEEE Trans. Biomed. Eng.* **49** 597–604
- [15] Sullivan T J, Deiss S R, Tzyy-Ping J and Cauwenberghs G 2008 A brain-machine interface using dry-contact, low-noise EEG sensors *ISCAS 2008: IEEE Int. Symp. on Circuits and Systems* pp 1986–9
- [16] Choi S-O 2007 An electrically active microneedle electroporation array for intracellular delivery of biomolecules *PhD Dissertation* School of Electrical and Computer Engineering, Georgia Institute of Technology, Atlanta, GA
- [17] Lorenz H, Despont M, Vettiger P and Renaud P 1998 Fabrication of photoplastic high-aspect ratio microparts and micromolds using SU-8 UV resist *Microsyst. Technol.* **4** 143–6
- [18] Bohl B, Steger R, Zengerle R and Koltay P 2005 Multi-layer SU-8 lift-off technology for microfluidic devices *J. Micromech. Microeng.* **15** 1125–30
- [19] Lorenz H, Despont M, Fahrni N, Brugger J, Vettiger P and Renaud P 1998 High-aspect-ratio, ultrathick, negative-tone near-UV photoresist and its applications for MEMS *Sensors Actuators A* **64** 33–9
- [20] Juncker D, Schmid H, Bernard A, Caelen I, Michel B, de Rooij N and Delamarche E 2001 Soft and rigid two-level microfluidic networks for patterning surfaces *J. Micromech. Microeng.* **11** 532–41
- [21] Yoon Y K, Park J H and Allen M G 2006 Multidirectional UV lithography for complex 3-D MEMS structures *J. Microelectromech. Syst.* **15** 1121–30
- [22] Choi S-O, Rajaraman S, Yoon Y-K, Wu X and Allen M G 2006 3D metal patterned microstructure using inclined UV exposure and metal transfer micromolding technology *Solid-State Sensor, Actuator, and Microsystems Workshop (Hilton Head 2006)* (Hilton Head, SC)
- [23] Garra J, Long T, Currie J, White S T R and Paranjape M 2002 Dry etching of polydimethylsiloxane for microfluidic systems *J. Vac. Sci. Technol. A* **20** 975–82
- [24] Hur S H, Khang D Y, Kocabas C and Rogers J A 2004 Nanotransfer printing by use of noncovalent surface forces: applications to thin-film transistors that use single-walled carbon nanotube networks and semiconducting polymers *Appl. Phys. Lett.* **85** 5730–2
- [25] Bao L R, Tan L, Huang X D, Kong Y P, Guo L J, Pang S W and Yee A F 2003 Polymer inking as a micro- and nanopatterning technique *J. Vac. Sci. Technol. B* **21** 2749–54
- [26] Zhao Y, Yoon Y-K, Choi S-O, Wu X, Liu Z and Allen M G 2009 Three-dimensional metal pattern transfer for replica molded microstructures *Appl. Phys. Lett.* **94** 023301
- [27] Park J-H, Yoon Y-K, Choi S-O, Prausnitz M R and Allen M G 2007 Tapered conical polymer microneedles fabricated by an integrated lens technique for transdermal drug delivery *IEEE Trans. Biomed. Eng.* **54** 903–13
- [28] Basmajian J V and DeLuca C J 1985 *Muscles Alive* (Baltimore, MD: Williams & Wilkins)
- [29] Cramer J T, Housh T J, Johnson G O, Ebersole K T, Perry S R and Bull A J 2000 Mechanomyographic and electromyographic responses of the superficial muscles of the quadriceps femoris during maximal, concentric isokinetic muscle actions *Isokinet. Exerc. Sci.* **8** 109–17
- [30] Huang C-N, Chen C-H and Chung H-Y 2004 The review of applications and measurements in facial electromyography *J. Med. Biol. Eng.* **25** 15–20
- [31] White J C, Hansen S R and Johnson R K 1988 A comparison of EMG procedures in the carpal tunnel syndrome with clinical-EMG correlations *Muscle Nerve* **11** 1177–82
- [32] Huigen E, Peper A and Grimbergen C A 2002 Investigation into the origin of the noise of surface electrodes *Med. Biol. Eng. Comput.* **40** 332–8